SPECTRUM OF ENGINEERING SCIENCES
ISSN (E) 3007-3138 (P) 3007-312X VOLUME 4, ISSUE 3, 2026

SUSTAINABLE CONSTRUCTION MATERIALS AND STRUCTURAL ANALYSIS FOR EARTHQUAKE-RESISTANT INFRASTRUCTURE: A MULTI-METHOD ASSESSMENT OF LOW-CARBON CONCRETE MIXES IN A MID-RISE REINFORCED-CONCRETE FRAME

Usama Tariq Javed[*1], Manazir Hussain[2], Hizza Qamar[3], Faisal Iqbal[4]

*[*1]National College of Business Administration and Economics (NCBA&E), Lahore, Pakistan*
[2] Department of Civil Engineering, University of Tokyo, Tokyo, Japan
[3] Urban and Regional Planning, National University of Sciences and Technology (NUST), Pakistan
[4]Bachelor in Civil Engineering Technology, Khwaja Fareed University of Engineering and Information Technology (KFUEIT), Rahim Yar Khan, Pakistan

[*1]usamatariqjaved54@gmail.com, [2]engr.manazir.hussain110@gmail.com, [3]hizzaqamar.hq@gmail.com, [4]faisaliqbalg7@gmail.com

DOI: https://doi.org/10.5281/zenodo.24034670

Keywords
Sustainable concrete; supplementary cementitious materials; embodied carbon; earthquake-resistant design; Eurocode 8; response-spectrum analysis; pushover; fragility; Monte Carlo; construction management; smart cities.

Article History
Received: 01 January 2026
Accepted: 16 March 2026
Published: 31 March 2026

Copyright @Author
Corresponding Author: *
Usama Tariq Javed

Abstract

Reinforced-concrete buildings in seismic regions must be both safe and low in embodied carbon, yet material studies and seismic studies are rarely combined. This paper links four concrete mixes (an OPC control, 30% fly ash, 50% ground granulated blast-furnace slag, and a ternary fly-ash/silica-fume blend) to the seismic assessment of a five-storey, three-bay reinforced-concrete frame. Material properties and emission factors are assumed within literature ranges; the structure is idealised as a five-degree-of-freedom shear building and analysed by modal response-spectrum analysis (Eurocode 8, ground type C, a_g = 0.30 g, q = 3.9), elastic time-history analysis with 24 synthetic records, pushover analysis, fragility analysis and Monte Carlo simulation, followed by cost estimation and multi-criteria ranking. Cement replacement lowered the embodied CO_2 of the concrete by 28.7%, 44.6% and 36.5%, and the embodied CO_2 of the whole frame (450 mm columns) by 19.5%, 30.2% and 24.8%. The fundamental period varied only between 0.572 and 0.588 s, so base shear was identical across mixes, and the code relation chosen for the elastic modulus (Eurocode 2 versus ACI 318) changed peak drift by about 16%, far more than the mix. Column size, cracked stiffness and storey height dominated drift sensitivity. For a section sized near the drift limit, strength variability (COV 15%) gave exceedance probabilities of 56.6%, 73.0%, 56.6% and 16.6% for the four mixes, and the slower strength gain of the fly-ash mix lengthened the time to reach 70% of the 28-day strength from 3.6 to 7.5 days. A TOPSIS ranking favoured the ternary blend under all three weighting scenarios. All strengths, emission factors, costs and structural parameters are assumed or simulated, so the findings describe relative trends for a representative frame, not a specific building.

INTRODUCTION

Concrete is the most widely used construction material in the world, and the cement within it is responsible for a substantial share of global anthropogenic CO_2 emissions [1], [2], [3]. At the same time, large urban populations live in regions

where strong earthquakes are a recurrent hazard, and buildings there must resist lateral forces without collapse, limit damage to economically acceptable levels, and remain serviceable where possible [4], [5]. Infrastructure planners therefore face a practical tension: the stiff, heavy, ductile concrete frames that perform well in earthquakes are also among the most carbon-intensive structures to build.

A widely available way to reduce this footprint is to replace part of the Portland cement with supplementary cementitious materials (SCMs) such as fly ash, ground granulated blast-furnace slag (GGBS) and silica fume [6], [7], [8]. SCMs lower the clinker content per cubic metre, often improve durability, and alter early-age and long-term strength development [9], [10]. The structural consequences of such substitution are, however, rarely examined together with the seismic response of the building: a designer is told that a mix is "greener" but not what this does to period, force demand, drift or the probability of exceeding a performance limit.

Seismic assessment itself is not a single calculation. Practice combines linear response-spectrum analysis for design forces [4], [11], nonlinear static (pushover) analysis for strength and ductility [12], [13], time-history analysis for response variability [14], [15], and probabilistic fragility functions for risk communication [16], [17]. Each method embodies different assumptions, and a material choice that looks benign in one may matter in another. The decision problem is further complicated by uncertainty in concrete strength, in the modulus–strength relation, and in cracked stiffness [18], [19].

Beyond design, infrastructure is increasingly delivered and managed through building information models (BIM), maturity sensing and structural health monitoring, which are components of smart sustainable city platforms [20], [21], [22]. These tools make it possible to account for embodied carbon quantities during construction, to decide on formwork-stripping times from measured strength, and to track stiffness change after an earthquake [23], [24], [25]. Their link to material-level decisions has not been well demonstrated.

This paper addresses the gap through a transparent, reproducible simulation study that covers five subject areas: (1) green building and sustainable materials, (2) earthquake-resistant design, (3) concrete technology and mix design, (4) structural analysis and modelling, and (5) construction management and smart cities. The contributions are: (i) a mix-to-structure workflow that carries four SCM-based mixes through strength, modulus, carbon, cost and time-dependent strength to a structural model; (ii) a multi-method seismic assessment (modal response-spectrum, time-history, pushover and fragility) of a mid-rise frame for each mix; (iii) global sensitivity and Monte Carlo analyses that expose which parameters actually control drift and carbon; (iv) a cost–carbon–performance ranking using TOPSIS [26]; and (v) a discussion that connects the results to construction management and monitoring. Section 2 reviews the literature, Section 3 states the research gap and objectives, Section 4 describes the methodology, Section 5 reports the results, Section 6 discusses them, Section 7 lists limitations and Section 8 concludes.

2. Literature Review

2.1 Green building and sustainable materials

Comprehensive reviews of low-carbon cement and concrete agree that no single measure will decarbonise the sector: clinker substitution, efficient design and use, alternative binders and carbon capture all contribute, with SCM substitution the most readily deployable at scale [2], [3], [27]. Miller et al. estimated that techniques already available could cut annual emissions from concrete production by more than 20% [6], and later commentary stressed that material efficiency in design is as important as binder chemistry [7]. Early work on "low-CO_2" cements had already pointed out the limits of substitution imposed by SCM availability and by early strength [28].

Life-cycle assessment (LCA) frameworks such as ISO 14040 and EN 15978 define how the environmental performance of a building or material should be assessed, with modules A1–A3 (product stage) typically dominating for structural concrete [29], [30]. Public inventories such as the ICE database provide the emission factors needed for such calculations, although values vary by

country, plant and allocation method [31]. Recycled aggregates offer a complementary route but affect stiffness and shrinkage, so their structural use needs care [32]. In this study the assessment is restricted to the product stage, which is where the choice among SCM mixes has its main effect.

2.2 SCM concretes and mix design

SCMs act through pozzolanic and latent-hydraulic reactions that refine pore structure and enhance durability, while slowing early strength development at high replacement levels [8], [9]. Practical replacement levels and performance data for fly ash, slag and silica fume are summarised by Thomas [10], and the physical basis of strength and stiffness development is given in standard references [33], [34]. Cement and concrete standards define permitted constituents, strength classes and conformity rules [35], [36], and mix proportioning follows established procedures based on target strength, water–binder ratio and workability [37].

Strength development with age is commonly modelled with the Eurocode 2 expression in which a coefficient s reflects cement class [38]; maturity-based methods can then convert measured temperature history to equivalent age and in-place strength [24]. The elastic modulus increases with strength but sub-linearly, and codes disagree on the relation: Eurocode 2 gives a secant modulus that is larger than the ACI 318 expression at the same nominal strength [38], [39]. This difference, often neglected, is shown in this paper to matter more for drift than the choice of SCM.

2.3 Earthquake-resistant design and performance-based engineering

Modern seismic design combines a design spectrum, a behaviour factor reflecting ductility and capacity-design rules that make beams yield before columns [4], [40], [41]. The spectral shapes used by codes descend from the work of Newmark and Hall [42], and detailing provisions draw on confinement research that explains how transverse reinforcement increases strain capacity [43]. Performance-based engineering extends this by linking demand to damage states, usually through drift, and by recognising that a code-compliant building may still sustain damage [5], [44].

Displacement-based design emphasises deformation rather than force, and its use of drift limits is closely related to the drift-based criteria adopted here [44]. Cumulative damage indices combine peak deformation and hysteretic energy [45], while resilience frameworks interpret performance in terms of recovery of function at community level [46], [47]. Innovative systems such as seismic isolation and structural control can reduce demand substantially, but their application depends on cost and building type [48], [49]. For regular mid-rise frames, which are the focus here, conventional ductile reinforced-concrete frames remain dominant [19], [41].

2.4 Structural analysis and modelling

Modal response-spectrum analysis is the standard linear method for regular multi-storey buildings; it requires mass and stiffness matrices to obtain periods, mode shapes and effective modal masses [11], [14]. Cracking reduces member stiffness, and codes allow a fraction of gross stiffness to be used in seismic analysis [4], [39]. Time-history analysis integrates the equations of motion using, for example, the Newmark average-acceleration scheme [15], and requires ground motions that are compatible with the design spectrum, which can be generated by filtered-noise models or selected from records [14], [17].

Nonlinear static analysis, as in the N2 method, estimates the capacity curve, overstrength and ductility and compares them with demand [12]; assessment standards give modelling parameters and acceptance criteria for existing and new buildings [13], [50]. Fragility functions, typically lognormal in intensity measure, express the probability of exceeding a damage state and can be fitted by incremental dynamic analysis, cloud analysis or simplified scaling [16], [17], [51]. For the present study, which is comparative, a simplified shear-building idealisation is used throughout so that differences between mixes are not obscured by modelling complexity.

2.5 Uncertainty, reliability and decision analysis

Concrete strength is variable even under good quality control, and structural reliability methods

treat it as a random variable, commonly with lognormal distribution and coefficients of variation of the order of 10–20% [18], [52]. Monte Carlo simulation propagates this variability through a deterministic model and provides exceedance probabilities [53]. When several criteria conflict, as with carbon, cost and performance, multi-criteria decision methods such as TOPSIS rank alternatives by closeness to an ideal solution [26]. Few studies have applied such methods to concrete mixes that are evaluated structurally rather than only materially [27].

2.6 Construction management and smart cities

BIM supports quantity take-off, scheduling, cost estimation and coordination, and has been linked to sustainability assessment because quantities can be combined with emission factors [20], [23]. On site, maturity sensing converts temperature history into estimated strength so that formwork can be removed when a target strength is reached, an important aspect when SCM concretes gain strength more slowly [24], [34]. Structural health monitoring uses measured vibration data to detect changes in natural frequency and mode shape that indicate damage [21], [25], [54].

At city scale, smart sustainable city frameworks emphasise data integration across infrastructure, with building condition, energy and resilience as interlinked dimensions [22], [55]. Resilience quantification for communities has been formalised in terms of robustness, redundancy, resourcefulness and rapidity [46], and infrastructure sustainability and resilience have been proposed as a unified problem [47]. These perspectives suggest that decisions about materials and structural systems should be informed by life-cycle carbon and by the ability to monitor and restore performance, which motivates the combined approach of this paper.

2.7 Summary of the literature

Table 1 summarises the main strands and the issues that remain open.

TABLE 1. Representative literature strands, main findings and open issues.

Theme	Sources	Main finding	Open issue
Low-carbon cement and concrete	[2], [3], [6], [28]	SCM substitution is the most deployable route to lower CO_2	Carbon benefit rarely carried into structural response
LCA and emission factors	[29], [30], [31]	Product stage dominates; factors vary by source	Sensitivity of frame carbon to factors seldom shown
SCM behaviour and mix design	[8], [9], [10], [37]	Slower early strength, better durability	Effect on stiffness and schedule not combined
Strength and modulus models	[34], [38], [39]	Modulus rises sub-linearly; codes differ	Code-model uncertainty vs mix effect unquantified
Seismic design and ductility	[4], [40], [41], [43]	Capacity design and confinement give ductility	Concrete class normally fixed in advance
Performance-based assessment	[5], [12], [13], [44]	Drift and deformation capacity govern damage	Few links to material choice
Dynamic analysis and fragility	[15], [16], [17], [51]	Lognormal fragilities from scaled dynamic analysis	Rarely compared across mixes
Uncertainty and decision analysis	[18], [26], [53]	Monte Carlo and TOPSIS handle variability and trade-offs	Rarely used with structural response of mixes
BIM, maturity and SHM	[20], [21], [24], [25]	Digital tools support quantities, strength and damage detection	Not connected to mix-level carbon decisions

Theme	Sources	Main finding	Open issue
Smart sustainable cities and resilience	[22], [46], [47], [55]	Resilience and data integration are core dimensions	Building-level material choices not linked

3. Research Gap and Objectives

3.1 Research gap

The review reveals five connected gaps. (G1) Studies of low-carbon concrete evaluate embodied carbon and material properties, but rarely propagate them into the seismic response of a structure [2], [27]. (G2) Seismic assessments typically fix the concrete class in advance, so the effect of substituting cement on period, force and drift is seldom quantified [4], [41]. (G3) The uncertainty of the modulus–strength relation across codes is rarely compared with the effect of the mix itself [38], [39]. (G4) Strength variability is treated through safety factors, and its effect on the probability of exceeding a drift limit is not shown for competing mixes [18], [53]. (G5) Construction-management and monitoring considerations, such as strength gain for formwork removal and sensing for post-event assessment, are discussed separately from material and structural design [21], [22], [24].

3.2 Research questions

The gaps lead to five research questions. RQ1: How much embodied carbon and cost can SCM-based mixes save in a reinforced-concrete frame, and how does this depend on the emission factors assumed [6], [31]? RQ2: Do these mixes change the period, base shear and drift of a mid-rise frame [4], [11]? RQ3: Which parameters control drift and carbon most strongly [18]? RQ4: How does strength variability change the probability of exceeding a drift limit and the fragility of the frame [16], [17]? RQ5: What do the results imply for construction scheduling, monitoring and smart-city decision platforms [20], [22]?

3.3 Objectives

The objectives are: (O1) to define four mixes and compute their assumed properties, embodied CO_2, cost and strength development [31], [37], [38]; (O2) to analyse a representative five-storey frame for each mix by modal response-spectrum analysis [4], [11]; (O3) to quantify the sensitivity of response and carbon to design and material parameters, including the code relation for modulus [39]; (O4) to cross-check the response-spectrum results with time-history and pushover analyses [12], [15]; (O5) to estimate exceedance probabilities and fragility curves under strength uncertainty [17], [53]; and (O6) to rank the mixes with a multi-criteria method and relate the findings to construction management and smart-city monitoring [26], [47].

3.4 Scope and novelty

The novelty lies in combining materials, seismic assessment, uncertainty and decision analysis in one reproducible framework, rather than in a new structural theory. The study is deliberately comparative: absolute values depend on assumed parameters, whereas the ordering of options and the relative size of effects are the main outputs [18], [44].

4. Methodology

4.1 Framework overview

Figure 1 shows how the five subject areas feed a common set of decision metrics. The workflow starts with mix proportions, from which strength, modulus, embodied CO_2, cost and strength gain are computed [31], [38]. These properties parameterise a structural model that is analysed by response-spectrum, time-history and pushover methods [4], [12], [15], followed by sensitivity, Monte Carlo, fragility and TOPSIS analyses [17], [26], [53]

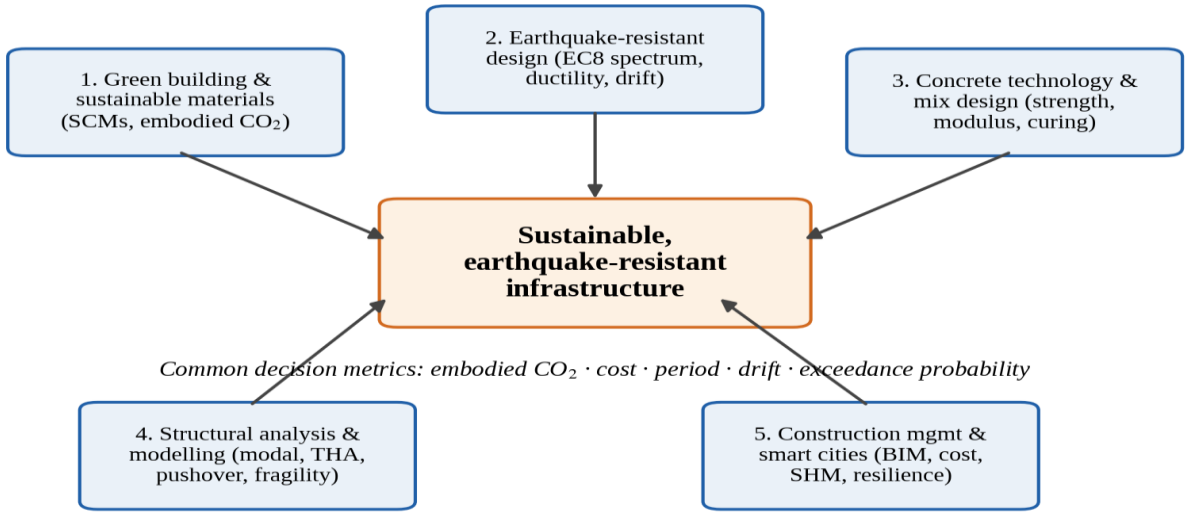


Fig. 1. Conceptual framework connecting the five subject areas through common decision metrics.

4.2 Concrete mixes

Four mixes with a total binder content of about 380 kg/m^3, a water–binder ratio of 0.45 (water 171 kg/m^3), coarse aggregate of 1050 kg/m^3 and fine aggregate of 780 kg/m^3 are considered, following the proportioning logic of ACI 211.1 and the constituent definitions of EN 197-1 and EN 206 [35], [36], [37]. M0 is a 100% OPC control; M1 replaces 30% of cement with fly ash; M2 replaces 50% with GGBS; and M3 is a ternary blend of 62% OPC, 30% fly ash and 8% silica fume. The characteristic cylinder strengths f_{ck} of 30, 28, 30 and 35 MPa are assumed to lie within the ranges reported for such binders [9], [10]; they are not laboratory measurements. Table 2 gives the proportions.

TABLE 2. Concrete mixes (kg/m^3) and assumed strength and strength-development parameter.

Mix	OPC	Fly ash	GGBS	Silica fume	f_{ck} (MPa)	s (EC2)
M0 OPC control	380	0	0	0	30	0.2
M1 30% fly ash	266	114	0	0	28	0.38
M2 50% GGBS	190	0	190	0	30	0.25
M3 ternary FA+SF	235	114	0	31	35	0.25

4.3 Material models, carbon and cost

The mean secant modulus is taken from Eurocode 2 [38], and a comparison is made with the ACI 318 expression [39]:

$$E_{cm} = 22[(f_{ck} + 8)/10]^{0.3}\ (GPa), \quad E_{ACI} = 4700\sqrt{f_{ck}}\ (MPa) \qquad (1)$$

Strength development with age t (days) follows the Eurocode 2 relation, in which the coefficient s depends on the cement or binder class [24], [38]:

$$f_{cm}(t) / f_{cm,28} = exp\{ s\,[1 - (28/t)^{1/2}] \} \qquad (2)$$

The time to reach 70% of the 28-day strength is used as a proxy for the earliest formwork-stripping time; this is a simplification because actual criteria depend on element type, loads and curing [24], [34]. Embodied CO_2 per cubic metre is the sum of constituent masses multiplied by emission factors, plus reinforcement [29], [31]:

$$e_c = \Sigma\, m_i\, \varepsilon_i + m_s\, \varepsilon_s \quad (3)$$

Assumed factors are 0.90 (OPC), 0.008 (fly ash), 0.07 (GGBS), 0.014 (silica fume), 0.0075 (coarse aggregate) and 0.005 (fine aggregate) kg CO_2/kg, and 1.4 kg CO_2/kg for steel at 120 kg/m^3 of concrete; transport, curing and construction-phase emissions are excluded [30], [31]. Unit costs (USD/kg) are 0.11 (OPC), 0.04 (fly ash), 0.085 (GGBS), 0.45 (silica fume), 0.015 and 0.014 (aggregates) and 1.8 for superplasticiser at 1.0–1.5% of binder; they are illustrative and market-dependent.

4.4 Structural model

The case structure is a regular five-storey reinforced-concrete frame with three 5 m bays in each direction (15 m × 15 m plan), a storey height of h = 3.2 m (total height 16 m) and sixteen square columns of width b. Each floor has a seismic weight of 2250 kN. As in simplified teaching and preliminary-design models, the frame is idealised as a shear building (Fig. 2) with lumped masses and storey stiffness [11], [14]:

$$k = n_c \cdot 12\, E\, c_r\, I / h^3, \quad I = b^4/12 \quad (4)$$

where n_c = 16 and c_r = 0.5 is the cracked-stiffness ratio recommended for concrete frames [4]. Beams are taken as rigid relative to columns, which is an upper-bound stiffness assumption [19]. Concrete volume is obtained from columns, beams (300 × 500 mm, eight 15 m lines per floor) and 200 mm slabs.

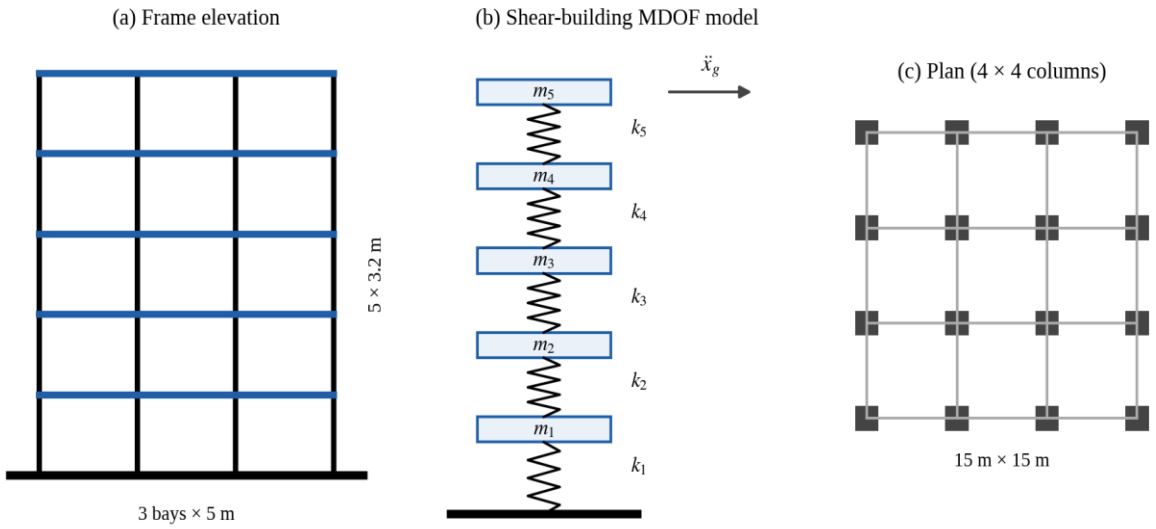


Fig. 2. Structural idealisation: (a) frame elevation, (b) shear-building multi-degree-of-freedom model, (c) floor plan.

4.5 Seismic action and response-spectrum analysis

The design spectrum is the Eurocode 8 Type 1 spectrum for ground type C (S = 1.15, T_B = 0.20 s, T_C = 0.60 s, T_D = 2.0 s) with design ground acceleration a_g = 0.30 g and behaviour factor q = 3.9, a value associated with medium-ductility frames [4]. The eigenproblem, modal participation and effective modal mass are:

$$K\,\varphi_j = \omega_j^2\, M\,\varphi_j, \quad \Gamma_j = \varphi_j^T\, M\, r \,/\, \varphi_j^T\, M\,\varphi_j, \quad M_{eff,j} = (\varphi_j^T\, M\, r)^2 \,/\, \varphi_j^T\, M\,\varphi_j \quad (5)$$

Modal base shears $V_{b,j} = M_{eff,j}\, S_d(T_j)$ are combined by the square-root-of-sum-of-squares rule over the first three modes [11]. Design displacements are obtained from the equal-displacement rule $d = q\, d_e$ [4], [12], and peak interstorey drift is the largest storey displacement difference divided by h. A design-level drift limit of 1.25% is adopted as a project criterion for comparison; it is not a code value. As a verification, the Eurocode 8 approximate period $T_1 = C_t H^{3/4}$ with C_t = 0.075 and H = 16 m gives 0.60 s, close to the computed value of 0.583 s for M0 with 450 mm columns [4];

the closed-form result for a uniform shear building, $\omega_1 = 2\sqrt{(k/m)}\sin[\pi/(2(2n+1))]$, reproduces the numerical eigenvalue [11].

4.6 Time-history analysis

To cross-check the response-spectrum results, 24 synthetic ground motions are generated by filtering white noise through a Kanai–Tajimi-type filter (ω_g = 15.6 rad/s, ζ_g = 0.6) and applying a Jennings-type envelope [14]. Each record is scaled so that its 5%-damped pseudo-acceleration at T_1 equals the elastic Eurocode 8 spectral value [4], [17]. Modal equations with 5% damping are integrated by the Newmark average-acceleration method [15], and floor displacements are reconstructed from five modes. This is an elastic comparison with the elastic response-spectrum value (q = 1), not an inelastic analysis.

4.7 Pushover and fragility analysis

A nonlinear static analysis is performed with an inverted-triangular lateral load pattern [12], [13]. Each storey is represented by an elastic–plastic shear spring with strain-hardening of 2% of the initial stiffness, equal columns over the height, and yield strength $V_y = 1.5\,V_{b,design}(f_{ck}/30)^{0.33}$; the exponent and overstrength are assumptions chosen to reflect the weak dependence of column capacity on concrete strength [19], [40]. The analysis ends when any storey drift reaches 2.5%. Ductility is estimated as $\mu = d_u/d_y^*$ with $d_y^* = V_{max}/K_0$ [12]. Fragility curves are lognormal [16], [17]:

$$P(D \geq d_{LS} \mid a) = \Phi[\ln(a/\theta_{LS})/\beta] \quad (6)$$

where θ_{LS} is the PGA at which the computed design drift equals the limit-state drift (0.5%, 1.0%, 1.5% and 2.5%, taken as slight, moderate, extensive and complete damage) and β = 0.40 combines record-to-record and modelling dispersion; the value is assumed [17], [51].

4.8 Sensitivity, Monte Carlo and decision analysis

One-at-a-time sensitivity of peak drift and frame carbon is evaluated by varying each parameter by ±20% around the base case [18]. Strength variability is modelled with lognormal f_{ck} (coefficient of variation 15%, unit-mean bias) and 800 Monte Carlo samples with common random numbers across mixes [52], [53]. Mixes are ranked by TOPSIS using five criteria: frame embodied CO_2 (minimise), concrete cost (minimise), elastic modulus (maximise), days to 70% strength (minimise) and drift-exceedance probability at 370 mm columns (minimise), with equal, carbon-led and performance-led weights [26].

4.9 Assumptions

TABLE 3. Principal parameters and assumptions.

Parameter	Value	Basis
Seismic action	EC8 Type 1, ground C, a_g = 0.30 g	Assumed [4]
Behaviour factor q	3.9 (sensitivity ±20%)	Assumed, ductile frame [4]
Geometry	5 storeys × 3.2 m; 3 × 3 bays of 5 m	Assumed
Floor seismic weight	2250 kN	Assumed
Cracked-stiffness ratio	0.5 (0.3–1.0 in sensitivity)	Code-permitted [4]
Elastic modulus	EC2 secant (ACI as check)	[38], [39]
Strength variability	Lognormal, COV 15%	Assumed [18]
Emission factors	As Section 4.3	Assumed, ICE-type [31]
Unit costs	As Section 4.3	Illustrative
Drift limit	1.25% design level	Project criterion
Pushover strength	$V_y = 1.5\,V_b(f_{ck}/30)^{0.33}$	Assumed [40]
Fragility dispersion	β = 0.40	Assumed [17]

5. Results

5.1 Mix properties, embodied carbon, cost and strength development

Replacing cement lowered the embodied CO_2 of the concrete from 353.8 kg/m^3 (M0) to 252.1 (M1), 196.1 (M2) and 224.6 kg/m^3 (M3), reductions of 28.7%, 44.6% and 36.5% (Fig. 3a). With reinforcement included, the reductions per cubic metre of reinforced concrete are smaller because steel contributes about 168 kg CO_2/m^3 for all mixes. Panel (b) shows the near-linear dependence of concrete carbon on replacement level, as expected when clinker dominates emissions [2], [6].

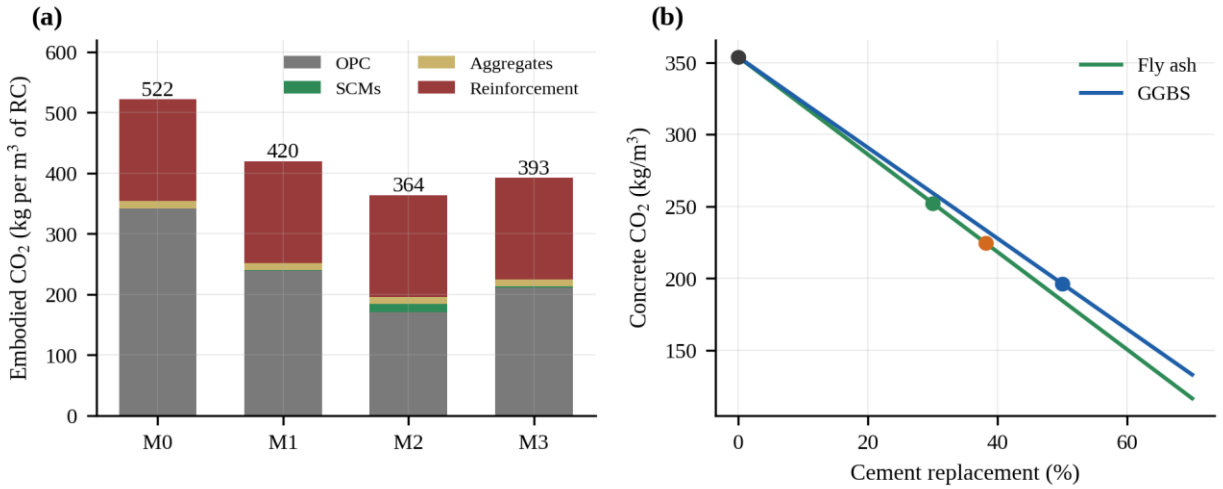


Fig. 3. Embodied CO_2: (a) breakdown by component for the four mixes; (b) concrete CO_2 versus cement replacement for fly ash and GGBS.

The elastic modulus ranged from 32.3 GPa (M1) to 34.1 GPa (M3) using the Eurocode 2 relation, but about 22% lower values are obtained with the ACI 318 expression at the same strength (Fig. 4a) [38], [39]. Strength development differed more clearly: the relative 7-day strength was 0.82 for M0 but 0.68 for M1, and the time to 70% of the 28-day strength rose from 3.6 days (M0) to 7.5 (M1), 4.8 (M2 and M3), while the 90-day gain was 1.18 for M1 against 1.09 for M0 (Fig. 4b) [9], [34]. Table 4 collects these properties together with cost.

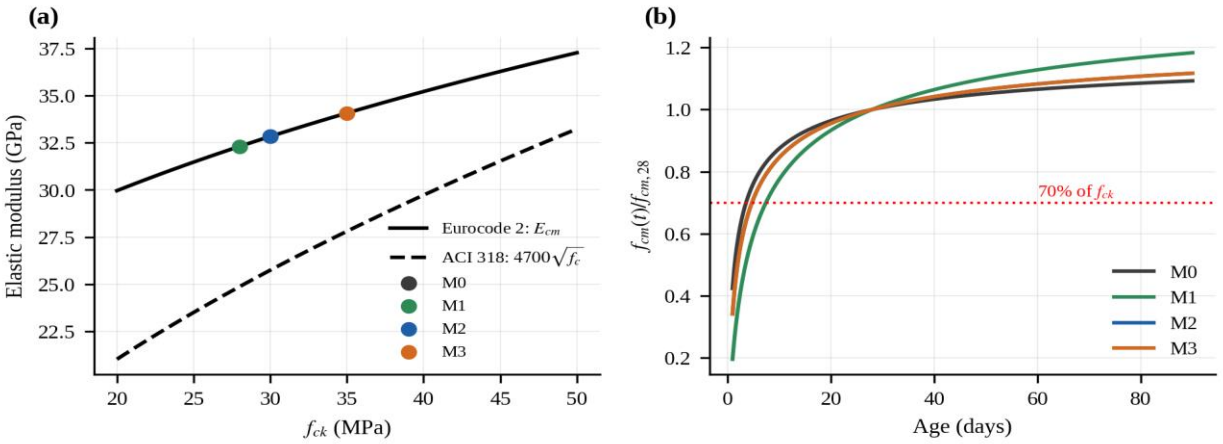


Fig. 4. Material behaviour: (a) elastic modulus versus characteristic strength for the Eurocode 2 and ACI 318 relations; (b) strength development with age.

TABLE 4. Mix properties, embodied carbon, cost and strength development.

Mix	f_{ck} (MPa)	E_{cm} (GPa)	CO_2 (kg/m^3)	Cost (USD/m^3)	f_7/f_{28}	Days to 70%	f_{90}/f_{28}
M0 OPC control	30	32.8	353.8	75.7	0.82	3.6	1.09
M1 30% fly ash	28	32.3	252.1	67.7	0.68	7.5	1.18
M2 50% GGBS	30	32.8	196.1	70.9	0.78	4.8	1.12
M3 ternary FA+SF	35	34.1	224.6	81.6	0.78	4.8	1.12

5.2 Dynamic properties and response-spectrum results

For 450 mm columns the fundamental period was 0.583 s for M0 and M2, 0.588 s for M1 and 0.572 s for M3, a spread below 3% (Fig. 5a, Table 5). The first mode carried 88% of the effective mass and the first three modes 99.1%, so the three-mode combination is adequate [11]. The first-mode shape (Fig. 5b) is nearly linear, typical of a shear building. All first periods lie on the spectrum plateau ($T_B \le T \le T_C$), so the design base shear was 2200 kN (coefficient 0.196) for every mix [4]; M0 and M2 are structurally identical because the same f_{ck} was assumed for them.

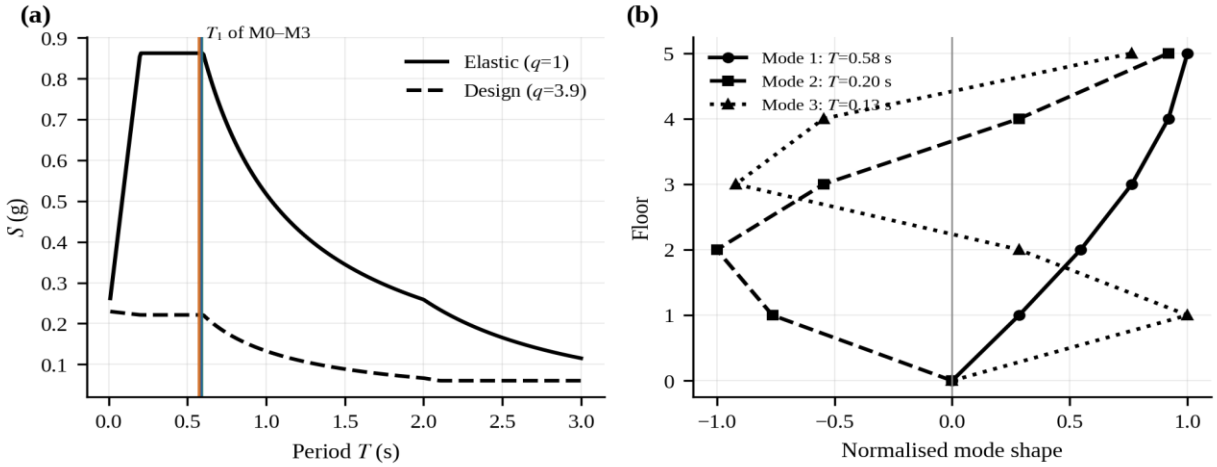


Fig. 5. Seismic characteristics: (a) elastic and design spectra with the fundamental periods of the four mixes; (b) first three mode shapes (M0, 450 mm columns).

TABLE 5. Modal properties and base shear for 450 mm columns.

Mix	T_1 (s)	T_2 (s)	T_3 (s)	$M_{eff,1}$ (%)	V_b (kN)	Max drift (%)
M0 OPC control	0.583	0.200	0.127	88.0	2200	0.82
M1 30% fly ash	0.588	0.201	0.128	88.0	2200	0.83
M2 50% GGBS	0.583	0.200	0.127	88.0	2200	0.82
M3 ternary FA+SF	0.572	0.196	0.124	88.0	2200	0.79

5.3 Drift profiles, section size and the carbon–drift trade-off

Storey drift decreased from the first to the top storey (Fig. 6a); for M0 the values were 0.82, 0.74, 0.62, 0.44, 0.23% from the first to the fifth storey, and the profile was almost identical for the other mixes. Roof displacement was about 91 mm (Fig. 6b). Peak drift fell sharply as columns became larger, from 1.06% at 400 mm to 0.37% at 550 mm for M0 (Table 6). The smallest column width meeting the 1.25% limit was 370 mm for M0, M2 and M3 and 375 mm for M1, so the stiffness

penalty of the fly-ash mix corresponds to about 5 mm of column width [44].

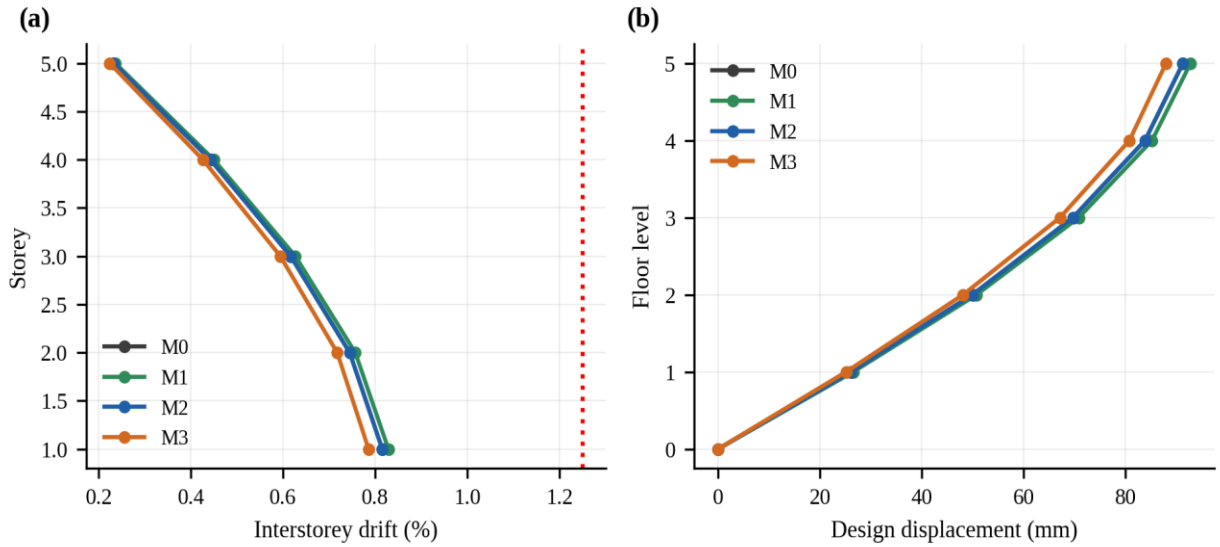


Fig. 6. Response profiles (450 mm columns): (a) interstorey drift by storey; (b) design displacement by floor level.

The carbon benefit of the mixes held at all column sizes (Fig. 7b): for 450 mm columns the frame embodied CO_2 fell from 172.6 t (M0) to 139.0, 120.5 and 129.9 t, reductions of 19.5%, 30.2% and 24.8%. Heat-map results for M0 (Fig. 7a) show that the combination of column width and cracked-stiffness ratio is what moves a design across the drift limit; mix choice shifts the curves by much less. At the minimum sections meeting the limit, frame CO_2 was 163.9, 132.3, 114.3, 123.3 t for M0–M3, respectively.

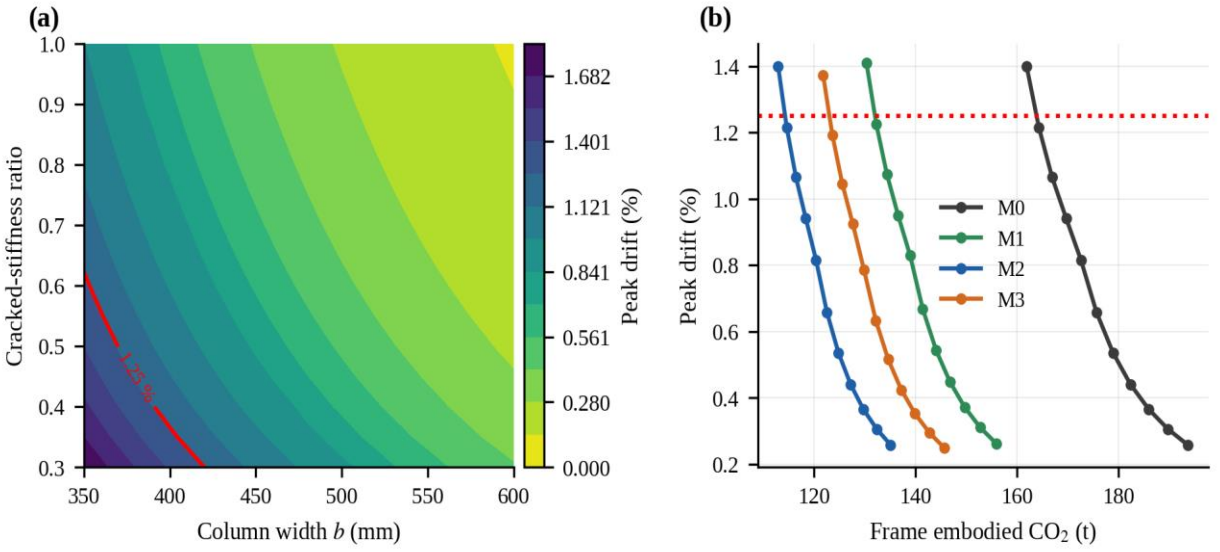


Fig. 7. Design space: (a) peak drift as a function of column width and cracked-stiffness ratio (M0), with the 1.25% limit; (b) peak drift versus frame embodied CO_2 for four column sizes per mix.

TABLE 6. Frame results for 450 mm columns and for the minimum section meeting the drift limit.

Mix	T_1 (s)	Drift (%)	Frame CO_2 (t)	b_{min} (mm)	Drift at b_{min} (%)	CO_2 at b_{min} (t)
M0 OPC control	0.583	0.82	172.6	370	1.25	163.9
M1 30% fly ash	0.588	0.83	139.0	375	1.22	132.3
M2 50% GGBS	0.583	0.82	120.5	370	1.25	114.3
M3 ternary FA+SF	0.572	0.79	129.9	370	1.22	123.3

5.4 Sensitivity analysis and code-model uncertainty

The one-at-a-time analysis (Fig. 8a) shows that peak drift is most sensitive to column width (62% to -52% for ±20% in b), followed by storey height, design acceleration, floor weight and cracked-stiffness ratio, whereas concrete strength changes drift by only about ±5% and the behaviour factor has no effect on design drift under the equal-displacement rule [4], [44]. For frame carbon (Fig. 8b), binder content and OPC emission factor were the dominant parameters (±11% for ±20%), followed by reinforcement quantity and factor (±8%), while the emission factors of SCMs were immaterial because they are small [6], [31]. The practical message is that the carbon result depends on the OPC emission factor adopted and should be stated alongside it [30].

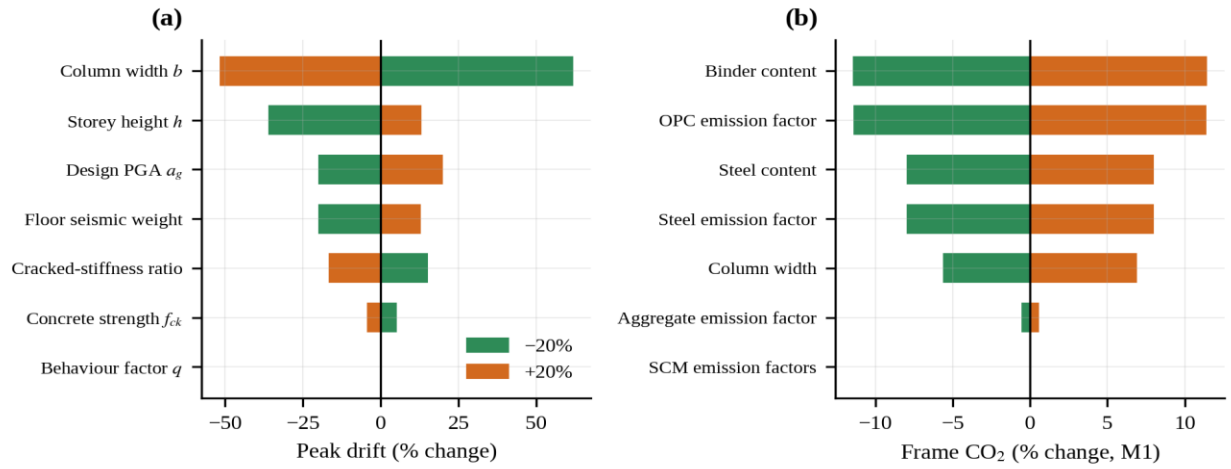


Fig. 8. One-at-a-time sensitivity (±20%): (a) peak drift for M0 at 450 mm; (b) frame embodied CO_2 for M1 at 450 mm.

The choice of modulus relation had a greater influence than the mix. Using $E = 4700\sqrt{f_{ck}}$ instead of the Eurocode 2 value increased T_1 from 0.583 to 0.659 s for M0 and peak drift from 0.82% to 0.95%, an increase of 16.3%; the corresponding drifts for M1–M3 were 0.97%, 0.95% and 0.91%. This difference exceeds the entire spread between mixes (0.79–0.83%) and is a reminder that code-model choice must be consistent with the aggregate type and test basis [19], [38], [39].

5.5 Time-history cross-check

Elastic time-history analysis of 24 spectrum-scaled records gave mean peak drifts of 0.82%, 0.83%, 0.82%, 0.79% for M0–M3, compared with 0.82%, 0.83%, 0.82%, 0.79% from the elastic response-spectrum analysis (Fig. 9b) [11], [15]. The agreement (within 2%) is expected because the first mode dominates and records were scaled at T_1; the dispersion across records was small (coefficient of variation about 3–4%) for the same reason, and would be larger with unscaled or

measured records [17], [51]. A representative record and roof response are shown in Fig. 9a.

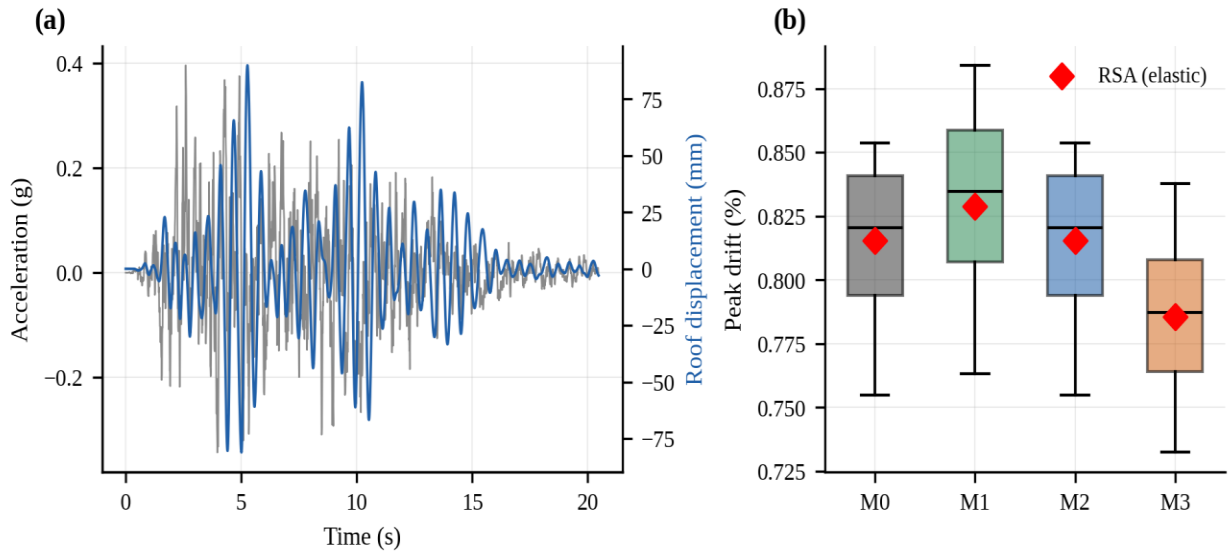


Fig. 9. Time-history check: (a) example synthetic record and roof displacement (M0); (b) distribution of peak drift over 24 records compared with the elastic response-spectrum result.

5.6 Pushover analysis

Capacity curves (Fig. 10a, Table 7) show an initial elastic branch and a hardening branch after the first-storey yield, because the columns are equal over the height while the storey shear is largest at the base [12], [40]. Drift therefore concentrates in the first storey (2.5% at ultimate against about 1.3% in the second storey, Fig. 10b), a weak-storey mechanism that limits global ductility to about 3.4 even though local storey ductility is higher [41], [44]. Overstrength relative to the design base shear ranged from 1.67 to 1.80, and the maximum base shear from 3680 to 3950 kN. These differences follow directly from the assumed strength–f_{ck} relation and should be treated as indicative only.

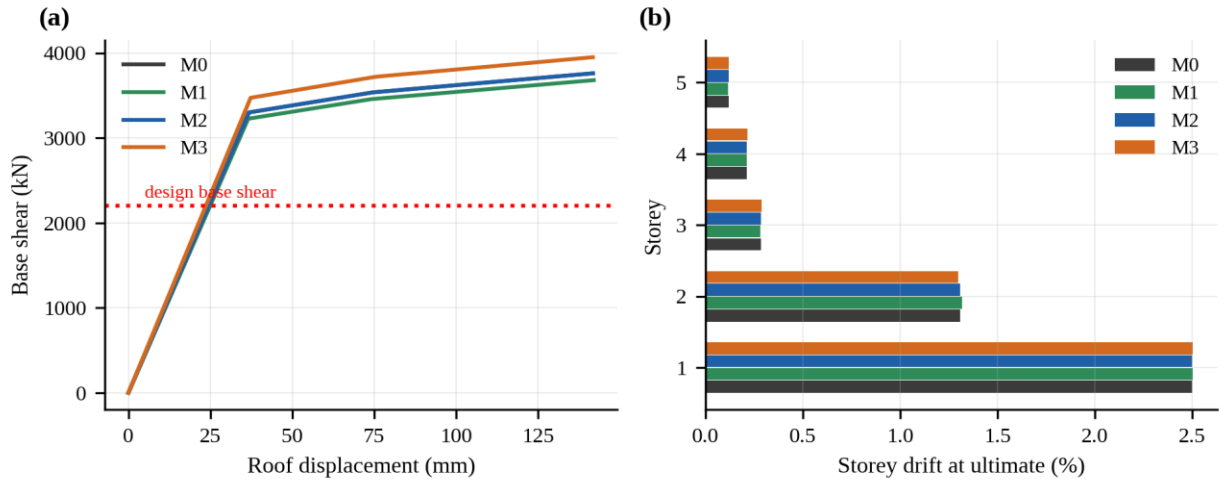


Fig. 10. Pushover results: (a) capacity curves for the four mixes with the design base shear; (b) storey drift at ultimate state.

TABLE 7. Pushover results (450 mm columns).

Mix	V_y (kN)	V_{max} (kN)	Overstrength Ω	d_y* (mm)	d_u (mm)	Ductility μ
M0 OPC control	3300	3760	1.71	42	142	3.38
M1 30% fly ash	3226	3680	1.67	42	142	3.41
M2 50% GGBS	3300	3760	1.71	42	142	3.38
M3 ternary FA+SF	3472	3950	1.80	42	142	3.34

5.7 Strength variability and exceedance probability

At 370 mm, close to the minimum section, the mean drift was 1.25%, 1.26%, 1.25%, 1.23% for M0–M3 and the probability of exceeding 1.25% was 56.6%, 73.0%, 56.6%, 16.6% (Fig. 11a, Table 8) [18], [53]. The standard deviation of drift was only about 0.02 percentage points, so the probability changes abruptly with section size: it fell from near 100% at 350–360 mm to zero at 380 mm for all mixes (Fig. 11b). Probability of exceedance is therefore a steep function of design margin, and a design sized to the limit has little reliability margin regardless of the mix. The higher-strength ternary mix gave the lowest exceedance probability at 370 mm because its modulus is higher.

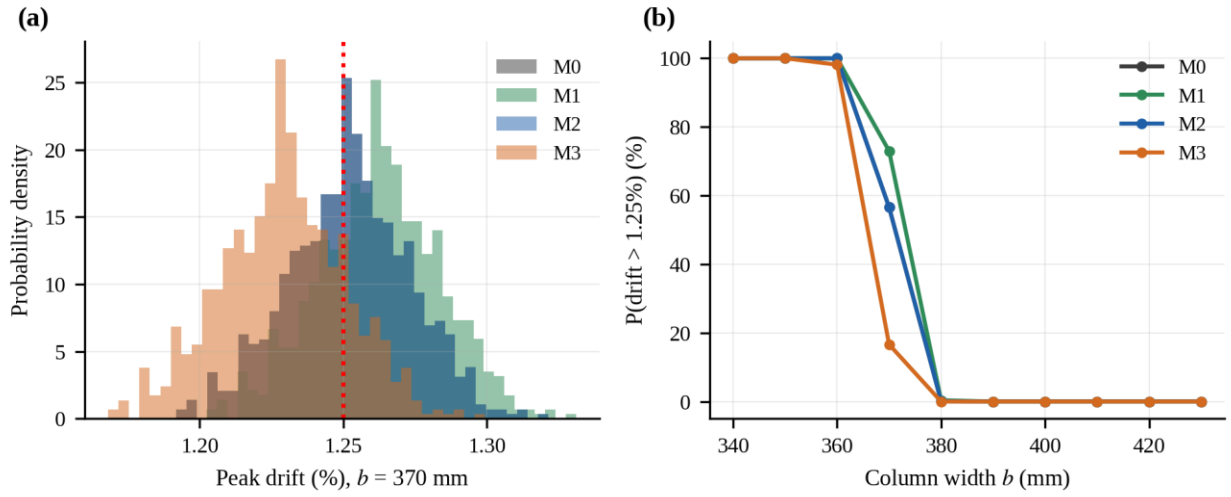


Fig. 11. Monte Carlo results (COV of f_{ck} = 15%): (a) distribution of peak drift at 370 mm; (b) drift-exceedance probability versus column width.

TABLE 8. Monte Carlo results at 370 mm columns (800 samples).

Mix	Mean drift (%)	Std. dev. (%)	95th percentile (%)	P(drift > 1.25%)
M0 OPC control	1.25	0.021	1.29	56.6%
M1 30% fly ash	1.26	0.021	1.30	73.0%
M2 50% GGBS	1.25	0.021	1.29	56.6%
M3 ternary FA+SF	1.23	0.022	1.26	16.6%

5.8 Fragility analysis

Median PGA capacities for the four limit states at 400 mm columns were 0.14, 0.28, 0.42, 0.70 g for M0 (Fig. 12a, Table 9) [16], [17]. At the design acceleration of 0.30 g the probability of exceeding the moderate-damage state (1.0% drift) was 56.3%

for M0 and 54.4% for M3, and of reaching the complete state (2.5%) 1.6% and 1.5% (Fig. 12b). The fragilities of the four mixes are almost indistinguishable at the scale of the figure, confirming that the mix has a minor influence on seismic risk relative to the structural section [51]. The relatively high probability of moderate damage at the design level is a consequence of the small section (400 mm) and the project drift criteria, and is not a statement about code-compliant buildings.

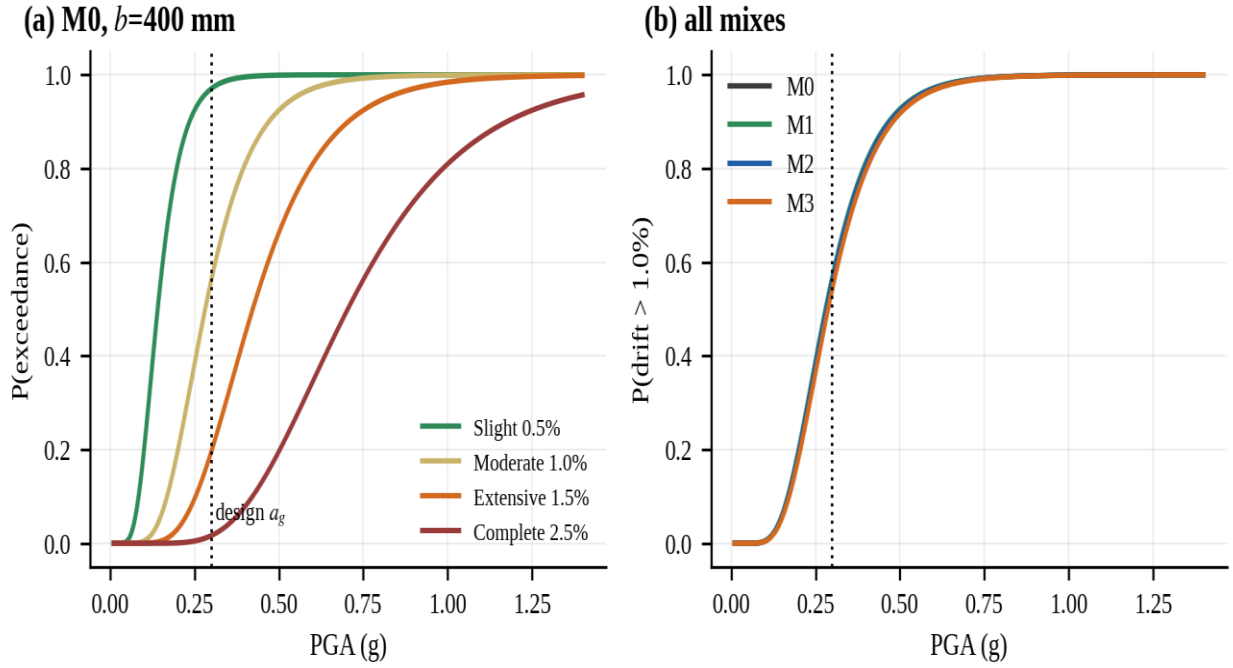


Fig. 12. Fragility curves (400 mm columns, β = 0.40): (a) four damage states for M0; (b) probability of exceeding 1.0% drift for the four mixes.

TABLE 9. Median PGA capacity (g) and exceedance probability at a_g = 0.30 g (400 mm columns).

Mix	$\theta_{0.5\%}$	$\theta_{1.0\%}$	$\theta_{1.5\%}$	$\theta_{2.5\%}$	P(≥1.0%)	P(≥1.5%)	P(≥2.5%)
M0 OPC control	0.14	0.28	0.42	0.70	56.3%	19.6%	1.6%
M1 30% fly ash	0.14	0.28	0.42	0.70	57.1%	20.2%	1.7%
M2 50% GGBS	0.14	0.28	0.42	0.70	56.3%	19.6%	1.6%
M3 ternary FA+SF	0.14	0.29	0.43	0.72	54.4%	18.3%	1.5%

5.9 Cost, carbon and multi-criteria ranking

Estimated concrete cost for the frame (450 mm columns) was USD 25029, 22389, 23457, 27007 for M0–M3 under the assumed unit prices (Fig. 13a). M1 and M2 were cheaper than the control because fly ash and slag cost less than cement, giving implied abatement costs of USD -78 and -30 per tonne of CO_2 (negative values mean savings), while M3 cost more because of silica fume, at about USD 46 per tonne of CO_2 avoided [6], [27]. The TOPSIS closeness scores (Fig. 13b, Table 10) ranked M3 first in all three weighting scenarios (0.80, 0.83, 0.85), mainly because its higher modulus and lower exceedance probability outweighed its higher cost; M1 was ranked last because of slower strength gain and the highest exceedance probability [26]. This ranking depends on including the near-limit exceedance criterion and on illustrative prices, and would change with local cost data or a larger design margin.

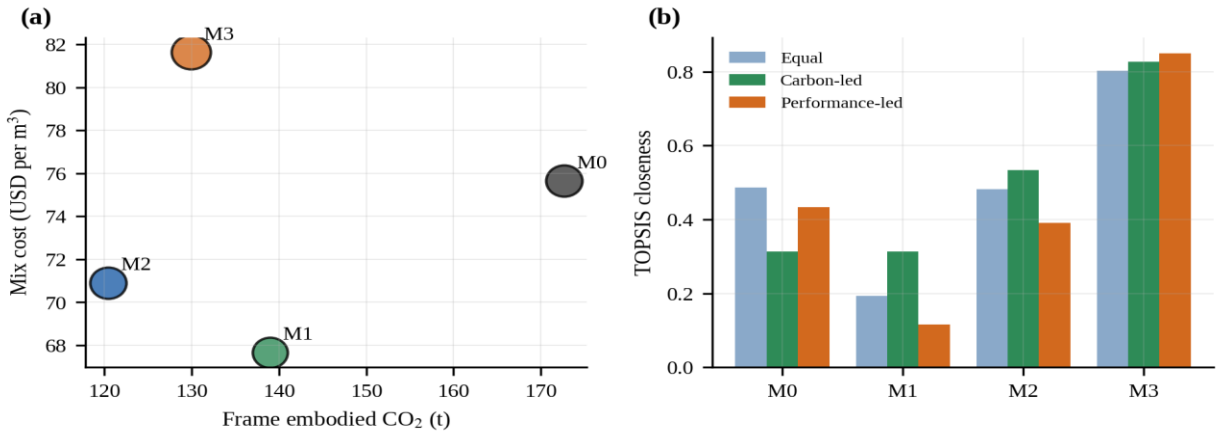


Fig. 13. Decision analysis: (a) mix cost versus frame embodied CO_2 (marker size scales with f_{ck}); (b) TOPSIS closeness under three weighting scenarios.

TABLE 10. TOPSIS criteria (450 mm columns) and closeness scores. Exceedance probability is for 370 mm columns.

Mix	CO_2 (t)	Cost (USD)	E (GPa)	Days to 70%	P_{exc}	Equal	Carbon-led	Perf.-led
M0 OPC control	172.6	25029	32.8	3.6	56.6%	0.49	0.31	0.43
M1 30% fly ash	139.0	22389	32.3	7.5	73.0%	0.19	0.31	0.12
M2 50% GGBS	120.5	23457	32.8	4.8	56.6%	0.48	0.53	0.39
M3 ternary FA+SF	129.9	27007	34.1	4.8	16.6%	0.80	0.83	0.85

IEER
Institute for Excellence in Education & Research

6. Discussion

6.1 Materials versus structure

The central finding is that, for this frame and these assumptions, the choice of cement-replacement mix has a large effect on embodied carbon and a small effect on seismic response. This follows from the weak dependence of elastic modulus on strength: a change in f_{ck} from 28 to 35 MPa raises E_{cm} by about 5.5% and shortens the period by about 3% [34], [38]. By contrast, geometric and modelling choices (column width, storey height, cracked stiffness and the modulus relation) change drift by tens of percent, in agreement with the emphasis on stiffness and deformation in displacement-based approaches [19], [44]. For designers, this means that SCM substitution can be pursued without redesigning the lateral system, provided that the strength and stiffness assumed in design are verified [4], [38].

6.2 Design implications

Three implications follow. First, cement replacement of 30–50% reduced frame embodied carbon by roughly 20–30% at the same section size, which is of the same order as reductions discussed for the concrete sector as a whole [2], [6]. Second, designs sized at the drift limit have almost no reliability margin, and the exceedance probability changes from near zero to near 100% over a 20–30 mm change in column width; this suggests adopting a deliberate margin rather than relying on mean properties [18], [53]. Third, the pushover results indicate that the weak-storey mechanism, not the mix, limits global ductility, which is consistent with capacity-design principles that require strong-column/weak-beam behaviour and uniform strength distribution [40], [41], [43].

6.3 Construction management implications

Slower strength gain of fly-ash mixes lengthened the time to 70% strength from 3.6 to 7.5 days in

the model, which may affect formwork-stripping times and floor-cycle durations; maturity sensing and in-place strength estimation can mitigate this by replacing fixed waiting times with measured strength [24], [34]. BIM quantity take-off can be coupled with the emission factors in Section 4.3 to produce embodied-carbon estimates as design options change, and costs from the same quantities enable the carbon–cost trade-off shown in Fig. 13 [20], [23]. Because the benefit depends on the emission factor of OPC (Fig. 8b), the factor source should be recorded as part of the model [30], [31].

6.4 Smart-city and monitoring implications

Figure 14 outlines how the results could be embedded in a monitoring and decision platform: sensors during construction (maturity probes) and operation (accelerometers) feed a digital twin that combines the BIM model, the structural model and a carbon ledger, and analytics modules estimate modal parameters, damage indices and fragility for city-scale resilience maps [21], [22], [46]. The stiffness range explored in this study corresponds to first-mode periods from 0.41 to 0.75 s, suggesting that frequency changes after damage would be measurable with standard accelerometers, as established in vibration-based damage detection research [25], [54]. At portfolio level, such information can be used to prioritise inspections and retrofit, and to link sustainability and resilience objectives in a single framework [47], [55].

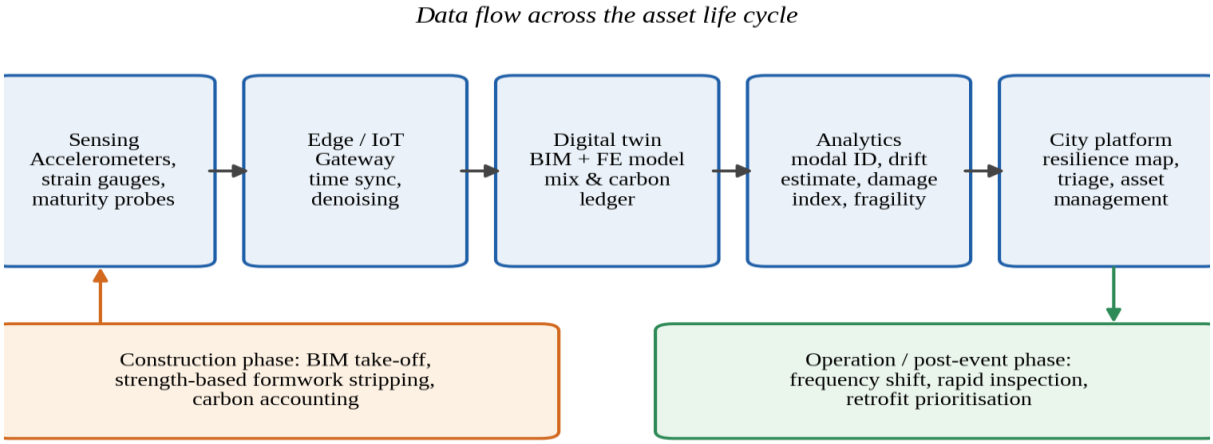


Fig. 14. Conceptual smart-city architecture linking construction-phase and operation-phase data to analytics and city-level decisions.

6.5 Comparison with earlier work

The findings are consistent with reviews that identify SCM substitution as a leading carbon-reduction measure with limited structural penalty when strength is maintained [2], [6], [27], and with code-based practice in which concrete strength class has a modest effect on frame stiffness [4], [41]. They add a quantitative comparison with code-model, geometric and modelling uncertainty that is not normally presented together with carbon, and illustrate how a single reproducible workflow can serve both the materials and the structural audience [17], [26]. Because the structural model is idealised, the results should be seen as a screening-level comparison rather than a substitute for detailed design [13].

6.6 Practical recommendations

Table 11 translates the findings into recommendations for designers and contractors. They are conditional on the assumptions of this study and should be checked against project-specific data and the applicable code [4], [39].

TABLE 11. Practical recommendations derived from the results.

Topic	Recommendation	Evidence
Mix selection	Use 30–50% cement replacement where strength at loading age is verified	Frame CO_2 reduced by about 20–30% [2], [6]
Stiffness assumptions	State the modulus relation and cracked-stiffness ratio explicitly and test sensitivity	Drift changed by about 16% between EC2 and ACI moduli [38], [39]
Section sizing	Provide a drift margin instead of sizing at the limit	Exceedance rose from near 0% to near 100% over 20–30 mm [18]
Ductility and detailing	Keep strength distribution uniform and apply capacity design to avoid a weak first storey	Drift concentrated in storey 1 in pushover [12], [40]
Construction scheduling	Use maturity sensing for formwork removal in slow-gaining mixes	Time to 70% strength rose from 3.6 to 7.5 days [24], [34]
Carbon reporting	Report emission-factor source and system boundary with every carbon figure	OPC factor changed frame CO_2 by ±11% [30], [31]
Monitoring	Install accelerometers in key buildings and track natural frequency	Period range 0.41–0.75 s for stiffness 1.0–0.3 [21], [25]

7. Limitations

The study is a simulation based on assumed values and has several limitations. Compressive strengths, strength-development coefficients, emission factors, unit costs, strength variability and the drift limit are not measured and were selected for illustration within literature ranges [10], [31]. The shear-building model neglects beam flexibility, torsion, joint deformation, soil–structure interaction and the contribution of infill walls [19], [41]. The equal-displacement rule and the elastic–plastic storey springs do not capture strength degradation, shear failure or the effect of confinement on deformation capacity [43], [45]. Time-history analysis used synthetic, spectrum-scaled records and was elastic, so it cannot assess inelastic dispersion [17], [51]. The pushover strength–f_{ck} relation and fragility dispersion are assumed. Durability, shrinkage, creep, long-term strength and carbonation were not modelled, and the carbon assessment is cradle-to-gate and excludes transport, construction and end-of-life modules [29], [30]. Monte Carlo analysis varied only strength and treated samples as independent, while real variability includes geometry, reinforcement and workmanship [18]. Results should be validated by laboratory testing, nonlinear analysis of a detailed model and a code-compliant design before use on a real project [4], [13].

8. Conclusion

This paper linked four low-carbon concrete mixes to a multi-method seismic assessment of a five-storey reinforced-concrete frame. The main conclusions are as follows. (1) Cement replacement cut concrete embodied CO_2 by 28.7%–44.6% and frame embodied CO_2 by 19.5%–30.2% at the same column size [2], [6]. (2) The mix changed the fundamental period by less than 3% and left the plateau-governed base shear unchanged, while the modulus relation (Eurocode 2 versus ACI 318) changed peak drift by about 16% [38], [39]. (3) Column size, storey height and cracked stiffness dominated drift sensitivity, and the behaviour factor did not affect design drift under the equal-displacement rule [4], [44]. (4) Time-history, pushover and fragility analyses supported the response-spectrum conclusions and showed that a weak-storey mechanism, not the mix, limits global ductility [12], [15], [17]. (5) Under 15% strength variability, a section sized at the drift limit had exceedance probabilities between 16.6% and 73.0% depending on the mix,

so a design margin and verified strength at loading age are needed [18], [53]. (6) Slower strength gain in fly-ash mixes affects the time to reach 70% strength, and maturity sensing and BIM-based carbon accounting can help manage this [20], [24]. (7) TOPSIS ranked the ternary blend first under all weighting scenarios, subject to the assumed prices and the near-limit exceedance criterion [26]. Future work will use laboratory-measured mix properties and long-term strength data, nonlinear time-history analysis of three-dimensional frame models with real ground motions, whole-life carbon assessment including transport and end-of-life, and field-calibrated BIM and monitoring data in a digital-twin demonstration [13], [21], [22], [51].

Data and Assumptions Statement

All results are generated by a parametric model whose parameters are listed in Sections 4.2–4.9 and Tables 2 and 3. No experimental or field data were used. The analysis scripts can be provided by the authors on reasonable request [53].

REFERENCES

[1] R. M. Andrew, "Global CO2 emissions from cement production, 1928–2018," Earth System Science Data, vol. 11, no. 4, pp. 1675–1710, 2019.

[2] K. L. Scrivener, V. M. John, and E. M. Gartner, "Eco-efficient cements: Potential economically viable solutions for a low-CO2 cement-based materials industry," Cement and Concrete Research, vol. 114, pp. 2–26, 2018.

[3] G. Habert et al., "Environmental impacts and decarbonization strategies in the cement and concrete industries," Nature Reviews Earth & Environment, vol. 1, pp. 559–573, 2020.

[4] EN 1998-1:2004, Eurocode 8: Design of structures for earthquake resistance – Part 1: General rules, seismic actions and rules for buildings. Brussels: CEN, 2004.

[5] A. Ghobarah, "Performance-based design in earthquake engineering: State of development," Engineering Structures, vol. 23, no. 8, pp. 878–884, 2001.

[6] S. A. Miller, A. Horvath, and P. J. M. Monteiro, "Readily implementable techniques can cut annual CO2 emissions from the production of concrete by over 20%," Environmental Research Letters, vol. 11, no. 7, art. 074029, 2016.

[7] P. J. M. Monteiro, S. A. Miller, and A. Horvath, "Towards sustainable concrete," Nature Materials, vol. 16, pp. 698–699, 2017.

[8] B. Lothenbach, K. Scrivener, and R. D. Hooton, "Supplementary cementitious materials," Cement and Concrete Research, vol. 41, no. 12, pp. 1244–1256, 2011.

[9] M. C. G. Juenger and R. Siddique, "Recent advances in understanding the role of supplementary cementitious materials in concrete," Cement and Concrete Research, vol. 78, pp. 71–80, 2015.

[10] M. Thomas, Supplementary Cementing Materials in Concrete. Boca Raton, FL, USA: CRC Press, 2013.

[11] A. K. Chopra, Dynamics of Structures: Theory and Applications to Earthquake Engineering, 5th ed. Hoboken, NJ, USA: Pearson, 2017.

[12] P. Fajfar, "A nonlinear analysis method for performance-based seismic design," Earthquake Spectra, vol. 16, no. 3, pp. 573–592, 2000.

[13] ASCE/SEI 41-17, Seismic Evaluation and Retrofit of Existing Buildings. Reston, VA, USA: American Society of Civil Engineers, 2017.

[14] R. W. Clough and J. Penzien, Dynamics of Structures, 3rd ed. Berkeley, CA, USA: Computers & Structures, Inc., 2003.

[15] N. M. Newmark, "A method of computation for structural dynamics," Journal of the Engineering Mechanics Division, ASCE, vol. 85, no. 3, pp. 67–94, 1959.

[16] C. A. Cornell, F. Jalayer, R. O. Hamburger, and D. A. Foutch, "Probabilistic basis for 2000 SAC Federal Emergency Management Agency steel moment frame guidelines," Journal of Structural Engineering, vol. 128, no. 4, pp. 526–533, 2002.

IEER Institute For Excellence in Education & Research

[17] J. W. Baker, "Efficient analytical fragility function fitting using dynamic structural analysis," Earthquake Spectra, vol. 31, no. 1, pp. 579–599, 2015.
[18] A. S. Nowak and K. R. Collins, Reliability of Structures, 2nd ed. Boca Raton, FL, USA: CRC Press, 2013.
[19] J. C. Wight and J. K. MacGregor, Reinforced Concrete: Mechanics and Design, 6th ed. Upper Saddle River, NJ, USA: Pearson, 2012.
[20] R. Sacks, C. Eastman, G. Lee, and P. Teicholz, BIM Handbook: A Guide to Building Information Modeling, 3rd ed. Hoboken, NJ, USA: Wiley, 2018.
[21] C. R. Farrar and K. Worden, Structural Health Monitoring: A Machine Learning Perspective. Chichester, UK: Wiley, 2013.
[22] S. E. Bibri and J. Krogstie, "Smart sustainable cities of the future: An extensive interdisciplinary literature review," Sustainable Cities and Society, vol. 31, pp. 183–212, 2017.
[23] S. Azhar, "Building information modeling (BIM): Trends, benefits, risks, and challenges for the AEC industry," Leadership and Management in Engineering, vol. 11, no. 3, pp. 241–252, 2011.
[24] N. J. Carino and H. S. Lew, "The maturity method: From theory to application," in Proc. Structures Congress & Exposition, ASCE, Washington, DC, USA, 2001.
[25] E. P. Carden and P. Fanning, "Vibration based condition monitoring: A review," Structural Health Monitoring, vol. 3, no. 4, pp. 355–377, 2004.
[26] C.-L. Hwang and K. Yoon, Multiple Attribute Decision Making: Methods and Applications. Berlin, Germany: Springer, 1981.
[27] J. de Brito and R. Kurda, "The past and future of sustainable concrete: A critical review and new strategies on cement-based materials," Journal of Cleaner Production, vol. 281, art. 123558, 2021.
[28] E. Gartner, "Industrially interesting approaches to 'low-CO2' cements," Cement and Concrete Research, vol. 34, no. 9, pp. 1489–1498, 2004.
[29] ISO 14040:2006, Environmental management – Life cycle assessment – Principles and framework. Geneva: International Organization for Standardization, 2006.
[30] EN 15978:2011, Sustainability of construction works – Assessment of environmental performance of buildings – Calculation method. Brussels: CEN, 2011.
[31] G. P. Hammond and C. I. Jones, Inventory of Carbon and Energy (ICE), Version 2.0. Bath, UK: University of Bath, 2011.
[32] R. V. Silva, J. de Brito, and R. K. Dhir, "Properties and composition of recycled aggregates from construction and demolition waste suitable for concrete production," Construction and Building Materials, vol. 65, pp. 201–217, 2014.
[33] P. K. Mehta and P. J. M. Monteiro, Concrete: Microstructure, Properties, and Materials, 4th ed. New York, NY, USA: McGraw-Hill, 2014.
[34] A. M. Neville, Properties of Concrete, 5th ed. Harlow, UK: Pearson, 2011.
[35] EN 197-1:2011, Cement – Part 1: Composition, specifications and conformity criteria for common cements. Brussels: CEN, 2011.
[36] EN 206:2013+A1:2016, Concrete – Specification, performance, production and conformity. Brussels: CEN, 2016.
[37] ACI Committee 211, Standard Practice for Selecting Proportions for Normal, Heavyweight, and Mass Concrete (ACI 211.1-91). Farmington Hills, MI, USA: American Concrete Institute, 1991.
[38] EN 1992-1-1:2004, Eurocode 2: Design of concrete structures – Part 1-1: General rules and rules for buildings. Brussels: CEN, 2004.
[39] ACI Committee 318, Building Code Requirements for Structural Concrete (ACI 318-19). Farmington Hills, MI, USA: American Concrete Institute, 2019.

IEER Institute for Excellence in Education & Research

[40] T. Paulay and M. J. N. Priestley, Seismic Design of Reinforced Concrete and Masonry Buildings. New York, NY, USA: Wiley, 1992.
[41] M. N. Fardis, Seismic Design, Assessment and Retrofitting of Concrete Buildings. Dordrecht, Netherlands: Springer, 2009.
[42] N. M. Newmark and W. J. Hall, Earthquake Spectra and Design. Berkeley, CA, USA: EERI, 1982.
[43] J. B. Mander, M. J. N. Priestley, and R. Park, "Theoretical stress-strain model for confined concrete," Journal of Structural Engineering, vol. 114, no. 8, pp. 1804–1826, 1988.
[44] M. J. N. Priestley, G. M. Calvi, and M. J. Kowalsky, Displacement-Based Seismic Design of Structures. Pavia, Italy: IUSS Press, 2007.
[45] Y.-J. Park and A. H.-S. Ang, "Mechanistic seismic damage model for reinforced concrete," Journal of Structural Engineering, vol. 111, no. 4, pp. 722–739, 1985.
[46] M. Bruneau et al., "A framework to quantitatively assess and enhance the seismic resilience of communities," Earthquake Spectra, vol. 19, no. 4, pp. 733–752, 2003.
[47] P. Bocchini, D. M. Frangopol, T. Ummenhofer, and T. Zinke, "Resilience and sustainability of civil infrastructure: Toward a unified approach," Journal of Infrastructure Systems, vol. 20, no. 2, art. 04014004, 2014.
[48] F. Naeim and J. M. Kelly, Design of Seismic Isolated Structures: From Theory to Practice. New York, NY, USA: Wiley, 1999.
[49] B. F. Spencer Jr. and S. Nagarajaiah, "State of the art of structural control," Journal of Structural Engineering, vol. 129, no. 7, pp. 845–856, 2003.
[50] ASCE/SEI 7-22, Minimum Design Loads and Associated Criteria for Buildings and Other Structures. Reston, VA, USA: American Society of Civil Engineers, 2022.
[51] D. Vamvatsikos and C. A. Cornell, "Incremental dynamic analysis," Earthquake Engineering & Structural Dynamics, vol. 31, no. 3, pp. 491–514, 2002.
[52] A. H.-S. Ang and W. H. Tang, Probability Concepts in Engineering: Emphasis on Applications to Civil and Environmental Engineering, 2nd ed. Hoboken, NJ, USA: Wiley, 2007.
[53] R. Y. Rubinstein and D. P. Kroese, Simulation and the Monte Carlo Method, 3rd ed. Hoboken, NJ, USA: Wiley, 2016.
[54] S. W. Doebling, C. R. Farrar, M. B. Prime, and D. W. Shevitz, "Damage identification and health monitoring of structural and mechanical systems from changes in their vibration characteristics: A literature review," Los Alamos National Laboratory, Rep. LA-13070-MS, 1996.
[55] V. Albino, U. Berardi, and R. M. Dangelico, "Smart cities: Definitions, dimensions, performance, and initiatives," Journal of Urban Technology, vol. 22, no. 1, pp. 3–21, 2015.

IEER
Institute for Excellence in Education & Research